Electrokinesis is a microbial behavior that requires extracellular electron transport

H. W. Harris[a], M. Y. El-Naggar[b], O. Bretschger[c], M. J. Ward[d], M. F. Romine[e], A. Y. Obraztsova[d], and K. H. Nealson[a,c,d,1]

[a]Department of Biological Sciences, University of Southern California, Los Angeles, CA 90089; [b]Department of Physics and Astronomy, University of Southern California, Los Angeles, CA 90089; [c]J. Craig Venter Institute, San Diego, CA 92121; [d]Department of Earth Sciences, University of Southern California, Los Angeles, CA 90089; and [e]Environmental and Molecular Sciences Laboratory, Pacific Northwest National Laboratory, Richland, WA 99352

Edited by E. Peter Greenberg, University of Washington, Seattle, WA, and approved November 11, 2009 (received for review July 4, 2009)

We report a previously undescribed bacterial behavior termed *electrokinesis*. This behavior was initially observed as a dramatic increase in cell swimming speed during reduction of solid MnO_2 particles by the dissimilatory metal-reducing bacterium *Shewanella oneidensis* MR-1. The same behavioral response was observed when cells were exposed to small positive applied potentials at the working electrode of a microelectrochemical cell and could be tuned by adjusting the potential on the working electrode. Electrokinesis was found to be different from both chemotaxis and galvanotaxis but was absent in mutants defective in electron transport to solid metal oxides. Using in situ video microscopy and cell tracking algorithms, we have quantified the response for different strains of *Shewanella* and shown that the response correlates with current-generating capacity in microbial fuel cells. The electrokinetic response was only exhibited by a subpopulation of cells closest to the MnO_2 particles or electrodes. In contrast, the addition of 1 mM 9,10-anthraquinone-2,6-disulfonic acid, a soluble electron shuttle, led to increases in motility in the entire population. Electrokinesis is defined as a behavioral response that requires functional extracellular electron transport and that is observed as an increase in cell swimming speeds and lengthened paths of motion that occur in the proximity of a redox active mineral surface or the working electrode of an electrochemical cell.

bacteria | microbial fuel cells | motility | chemotaxis | galvanotaxis

Shewanella species are widespread in nature, enjoying a cosmopolitan distribution in marine, freshwater, sedimentary, and soil environments (1). They have attracted considerable attention in recent years because of their ability to reduce an extensive number of different electron acceptors, including the solid (oxy)hydroxides of iron and manganese, such as $Fe(OH)_3$ and MnO_2, using one or more proposed mechanisms of extracellular electron transport (EET) (2, 3). The EET ability of *Shewanella* species is consistent with their ability to generate electric current in microbial fuel cells (MFCs) in the absence of exogenous electron shuttles (4). Various strategies of extracellular electron transfer have been proposed in metal-reducing microbes, including naturally occurring (2) or biogenic (5–7) soluble mediators that "shuttle" electrons from cells to acceptors, as well as direct transfer using multiheme cytochromes located on the cell exterior (8) and transfer via conductive nanowires (9–11).

S. oneidensis MR-1 features several proteins that are involved with the transport of electrons to the exterior of the cell, where they play an important role with regard to the reduction of solid electron acceptors such as metal oxides. These include two outer-membrane decaheme *c*-type cytochromes (MtrC and OmcA), a membrane-spanning protein (MtrB), and two periplasmic multiheme *c*-type cytochromes (MtrA and CymA). Deletion of the genes encoding any of these proteins leads to phenotypes that are greatly inhibited with regard to metal-oxide reduction and current production in MFCs (12, 13). The mutation of genes that code for proteins involved in the placement of cytochromes to the outer membrane also results in the loss of metal-reducing phenotypes (13).

The shewanellae are highly motile, by virtue of a single polar flagellum, and individual *S. oneidensis* MR-1 cells have been tracked swimming at speeds of up to, and sometimes more than, 100 μm/sec, although the average swimming speed of cells in a population is considerably lower (14). Research has also shown that *S. oneidensis* MR-1 displays chemotactic responses to several soluble electron acceptors, including Fe(III) citrate (15, 16), and that the CheA-3 histidine protein kinase is required for this chemotactic behavior (14). In the absence of an electron acceptor MR-1 cells stop swimming; however, motility can be restored upon the readdition of an electron acceptor.

Here we present data that suggest that the shewanellae exhibit a unique motility response: we call it *electrokinesis*. This response, which involves increased swimming speeds and prolonged runs, was observed when cells were in close proximity to a redox active surface, such as an MnO_2 particle, or the working electrode of an electrochemical cell. Cells in the presence of MnO_2 particles were frequently observed to touch the mineral surface and sometimes pause for up to 1 sec, before swimming away. Video microscopy showed a concomitant reduction of the MnO_2 particles, suggesting that electrokinesis could be associated with the use of insoluble surfaces as electron acceptors. Electrokinesis is not a uniform response that can be observed in all cells, although if an electron shuttle is added the proportion of cells swimming and the average swimming speed of these cells rapidly increased.

Results

Behavioral Responses of *S. oneidensis* MR-1 to Manganese and Iron Oxides. Initial microscopic observations of *S. oneidensis* MR-1 cells mixed with MnO_2 particles showed a population of highly motile cells around the solid phase electron acceptor particles. In contrast, MR-1 cells sealed into capillary tubes in the absence of MnO_2 particles eventually ceased swimming and exhibited only Brownian motion. The motility response, which we call electrokinesis, was localized to the areas surrounding the metal oxide particles and was coincident with the reduction and subsequent dissolution of the particles (the highly motile cells are shown in Movie S1 and Movie S2; reduction of an MnO_2 particle, during a 24-h experiment, is shown in Fig. 1*A* and Movie. S2). The swimming activity was quantified within the first 2 h of each experiment using video-microscopic observations coupled with cellular tracking algorithms that yielded cell positions, trajectories, and 2D maps of swimming speed (*Materials and Methods*). An analysis of the motility response in the presence of MnO_2 particles showed a dramatic increase in cell swimming velocity

Author contributions: H.W.H., M.Y.E.-N., O.B., A.O., and K.N. designed research; H.W.H. and O.B. performed research; M.F.R. contributed new reagents/analytic tools; H.W.H., M. Y.E.-N., O.B., M.J.W., M.F.R., A.O., and K.N. analyzed data; and H.W.H., M.Y.E.-N., M.J.W., and K.N. wrote the paper.

The authors declare no conflict of interest.

This article is a PNAS Direct Submission.

[1]To whom correspondence should be addressed: E-mail: knealson@usc.edu.

This article contains supporting information online at www.pnas.org/cgi/content/full/0907468107/DCSupplemental.

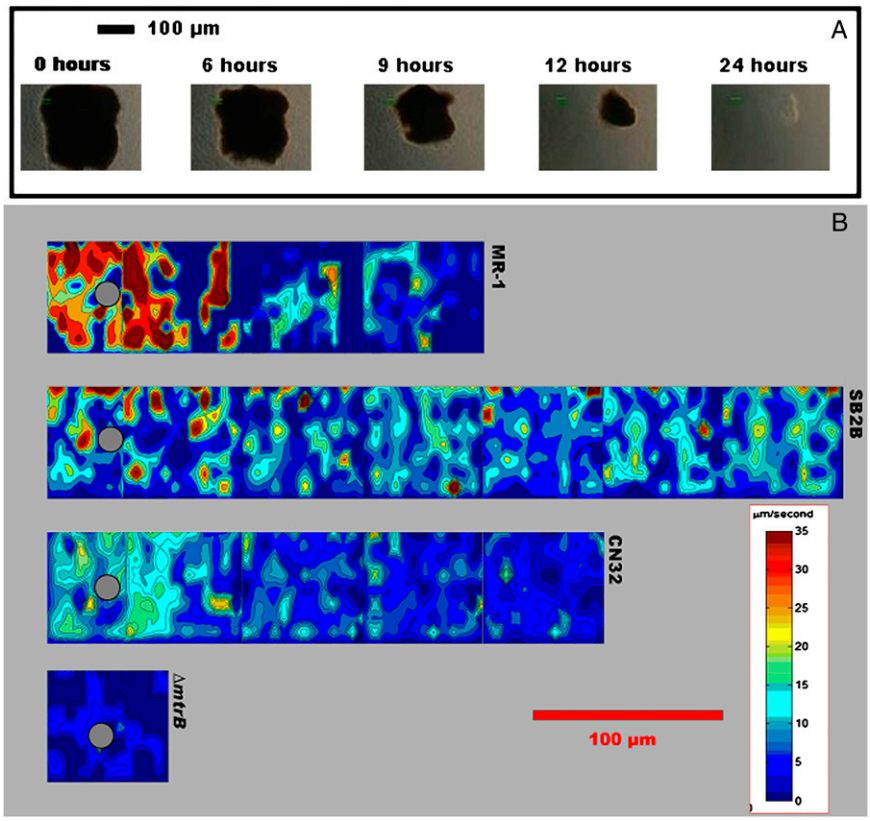

Fig. 1. Video microscopy photographs and motility analysis during bacterial reduction of MnO_2 particles. (*A*) Five frames from video data at 40× show the progressive reduction of a large (≈180 μm diameter) MnO_2 particle over the course of 24 h. Frames are displayed from initial (*Left*) to 24 h (*Right*) at denoted time intervals (0, 6, 9, 12, and 24 h). (*B*) Four contour plots of bacterial average velocity around similar-sized MnO_2 particles (*Left Center*), as calculated by our image analysis algorithm. The four representative experiments were conducted with strains *S. oneidensis* MR-1, *S. amazonensis* SB2B, *S. putrefaciens* CN32, and *S. oneidensis* MR-1 Δ*mtrB,* which are displayed from top to bottom in panoramic strips. These plots illustrate the correlation between motility near a MnO_2 particle and reduction of the particle. MR-1 and SB2B both reduced MnO_2 particles at a rapid pace (<24 h), whereas CN32 reduced at a much slower pace (>24 h) and the Δ*mtrB* mutant did not reduce at all. A number of 30-sec video clips are assembled in the panoramic strips. The contour maps show regions of high bacteria traffic (red) around the MnO_2 particles (denoted with gray circle).

close to the particles (Fig. 1*B*, *Top*). Prolonged run lengths were also observed (Fig. 2*B*). Cells were also frequently observed to touch the MnO_2 particles, sometimes pause for up to 1 sec, then swim away, suggesting that the motility response could be associated with the direct transfer of electrons to the mineral surface. When soluble electron acceptors (10 mM fumarate, 5 mM nitrate, or 10 mM thiosulfate) were added individually to anaerobic capillary tubes containing *S. oneidensis* MR-1 cells and MnO_2 particles, the fast-swimming motility response became uniform, rather than being localized around the MnO_2 particles.

Video-microscopic analysis was used to observe behavioral responses of *S. oneidensis* MR-1 cells in the presence of both MnO_2 and iron (oxy)hydroxide [$Fe(OH)_3$] particles. The data showed that kinetic responses to these anaerobic electron acceptors were distinct: in contrast to the MnO_2 particles, which evoked a strong response (i.e., a large number of fast-swimming cells were observed around the particle), $Fe(OH)_3$ particles elicited very subtle responses (i.e., few cells were observed swimming in the proximity of the particles, and these cells were, on average, swimming more slowly). Figure 2*A* and Movie S3 show the lack of swimming around $Fe(OH)_3$ particles, whereas Movie S4 shows the slow reduction of an $Fe(OH)_3$ particle. Because of this difference, our subsequent studies were performed with MnO_2 particles. The response to MnO_2 resulted in fast-swimming bacteria around the particle for the first 2 h of each experiment, followed by the eventual formation (over the next 24 h) of a biofilm. Cell tracking was not performed after the first 2 h of each experiment because at later times an accumulation of cells around the particles was observed (Movie S2). This accumulation was potentially caused by a chemotactic response to soluble Mn(II) gradients, generated during the reduction of the MnO_2 particles, and was not considered to be part of the electrokinetic response.

One important characteristic of the electrokinetic response was that it involved only a fraction of the population of MR-1 cells. Although the exact proportions of the cell populations that were swimming were difficult to quantify because of the 3D distribution of the bacteria, they seemed to range from zero to ≈35% of the cells in view near the MnO_2 particles. When cells were observed far from the MnO_2 particles but still inside the anaerobic capillary, they were uniformly nonmotile (Movie S5 is a panoramic view of the bacterial response around an MnO_2 particle). Nonmotile cells are still represented in our graphs as having nonzero velocity because our computer tracking algorithms recorded Brownian motion indiscriminately from swimming. However, because we could distinguish the region around the particles where bacterial swimming speeds were increased, from the region where cells showed Brownian motion alone, we noted "activity radii" around the particles, within which the behavioral change occurred (Table 1).

Electrokinesis Requires Extracellular Electron Transport. Our initial series of experiments suggested that electrokinesis could be associated with the use of MnO_2 as an anaerobic electron acceptor because the motility response occurred coincidentally with MnO_2 particle reduction, and because the cells were frequently observed to touch the mineral surface. Several *S. oneidensis* MR-1 mutants, including Δ*mtrA*, Δ*mtrB*, and Δ*cymA*, are unable to reduce MnO_2 during anaerobic respiration (13). These mutants were consequently screened in our assay for electrokinesis in response to the presence of MnO_2 particles. None of the mutants showed an increase in swimming speed or a notable activity radius around the MnO_2 particles (data shown in Table 1 and for the Δ*mtrB* mutant in Fig. 1*B*, *Bottom*). This result suggested that electrokinesis is dependent on EET and, consequently, that other extracellular electron acceptors, such as the graphite electrodes of MFCs, could also elicit electrokinesis.

Electrokinetic Responses to Graphite Electrodes. Electrokinesis was observed in *S. oneidensis* MR-1 cells exposed to the working electrode of a miniature electrochemical cell comprising two compartments separated by an ion-exchange membrane (Fig. S1).

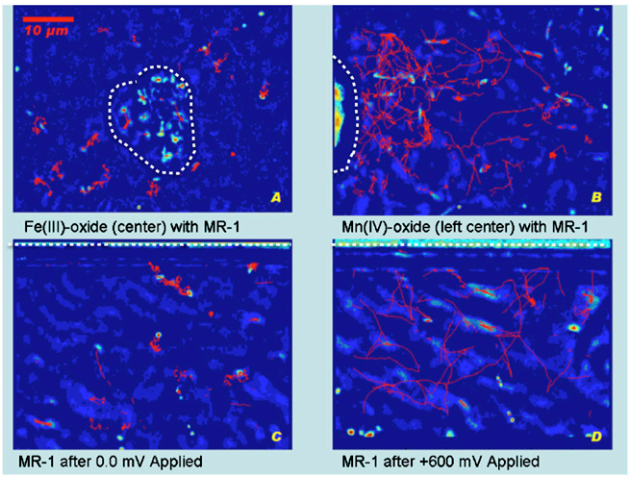

Fig. 2. Bacterial trajectories. Tracking trajectories (red lines) for *S. oneidensis* MR-1 cells during 10-sec video samples captured using 100× magnification. In all four experiments the bacteria are using 20 mM lactate as their carbon source. The strains were captured on video while sealed in anaerobic capillary tubes. (*A*) An $Fe(OH)_3$ particle (located in the center of the frame) elicited considerably less motility response than an MnO_2 particle (located left center) (*B*) where cells were observed swimming at speeds of 40–80 μm/sec. Touch-and-go behavior, in which the bacteria briefly contact the metal oxide surface, was observed for the next 2 h (Movie S1). (*C*) Trajectory diagram for 10 sec of video at 100× magnification adjacent to the working electrode. Video captured after MR-1 was exposed to 10 min at 0 mV vs. graphite reference electrode. (*D*) Video captured after MR-1 was exposed to 10 min at +600 mV. Swimming increased immediately (1–30 sec) after the voltage was applied, then continued to increase over the next 20 min. At 0 mV or any relatively lower voltage the motility activity decreased but returned when +600 mV was reapplied (Movie S6). Approximate boundaries of the mineral particles and the location of the graphite electrodes are shown by dashed white lines.

These electrode-based experiments offer the advantage of observing cells without interference from soluble metal species generated as a consequence of mineral dissolution [an important distinction because the Mn(II) and Fe(II) gradients generated during the reduction of Mn(III/IV)- and Fe(III)-containing minerals, respectively, have been suggested to elicit chemotactic responses in *S. oneidensis* MR-1 (16)]. Observations of MR-1 motility behavior in close proximity to a graphite electrode maintained at a positive potential (+600 mV vs. graphite reference electrode) identified behavior similar to that observed during MnO_2 particle reduction (Movie S6). MR-1 cells exhibited strong electrokinesis around the electrode with +600 mV applied potential (Fig. 2*D*, Fig. 3*A*, *Top*, and *B*, and Table 1), less response with +300 mV applied potential, and very limited response at negative or zero applied potentials (Fig. 2*C*, Fig. 3*B*, and Table 1). As with the MnO_2 particle reduction, fast swimming was confined to a small percentage of the cells in the vicinity of the electrode. Analysis of the Δ*mtrB*, Δ*mtrA*, and Δ*cymA* mutants again showed that electrokinesis in response to the working electrode potential was dependent on EET functionality (Table 1 and for the Δ*mtrB* mutant in Fig. 3*A*, *Bottom*, and *B*).

Electrokinesis Occurs Independent of Electron Shuttles. Our experiments with both MnO_2 particles and graphite electrodes showed that the electrokinetic response was always confined to a small percentage of the cell population. This restriction might not be expected if EET under these conditions was dependent on the presence of a soluble electron shuttle (which would make an electron acceptor available to all of the cells). The addition of 1 mM of an extracellular electron shuttle, 9,10-anthraquinone-2,6-disulfonic acid (AQDS), to a culture of MR-1 cells mixed with MnO_2 particles, induced the fast-swimming motility response in more than 90% of the cells (the average swimming speed of tracked cells increased from 9.1 ± 2.1 μm/sec to 23.7 ± 1.4 μm/sec), along with a more rapid reduction of the MnO_2 particles. An analysis of the Δ*mtrA* and Δ*mtrB* EET mutants showed that these mutants responded similarly to wild-type in the presence of both MnO_2 particles and AQDS (Table 1), even though a previous report indicated that a different *mtrB* mutant (DKN248) could not reduce AQDS (17). The reason for the differences in the *mtrB* mutants is unclear.

Electrokinesis Is Distinct from Chemotaxis and Galvanotaxis. The increase in cell swimming speed and the associated prolonged runs observed during electrokinesis suggested that this behavioral response was different from chemotaxis (which involves changes in the reversal frequency of cell swimming). To determine whether chemotaxis did play a role in the motility response to both the MnO_2 particles and the graphite electrode of our electrochemical cell, we tested the behavior of a *S. oneidensis* Δ*cheA-3* mutant. This mutant lacks a CheA histidine protein kinase that is essential for chemotactic signal transduction in *S. oneidensis* MR-1 (14). With changing applied potential the Δ*cheA-3* mutant responded similarly to MR-1. However, in the presence of MnO_2 particles the Δ*cheA-3* mutant cells were mostly nonmotile. The lack of a localized swimming population around the MnO_2 particles was potentially due to the smooth-swimming (nonstopping)

Table 1. Comparison of electrokinetic response to MFC current production in *Shewanella* strains and mutants

	Response to:							
	Electron acceptors (activity radii, μm)					Electrode (activity radii, μm)		
Shewanella strains/mutants	None	MnO_2	$Fe(OH)_3$	MnO_2 + AQDS	$Fe(OH)_3$ + AQDS	0 mV	+600 mV	Current production (relative to MR-1)
S. oneidensis MR-1	nr	<200	nr	<550	<350	nr	100–200	++
MR-1 Δ*cheA3*	nr	nr	nr	<550	<400	nr	100–200	+++
MR-1 Δ*cymA*	nr	nr	nr	nd	nd	nr	nr	—
MR-1 Δ*mtrA*	nr	nr	nr	<550	<450	nr	nr	—
MR-1 Δ*mtrB*	nr	nr	nr	<550	<450	nr	nr	—
S. amazonensis SB2B	nr	<450	nr	nd	nd	nr	100–200	++
S. putrefaciens CN32	nr	<250	nr	nd	nd	nr	<100	+

nr, no or negligible response; nd, not determined; ++, current production of wild-type MR-1.

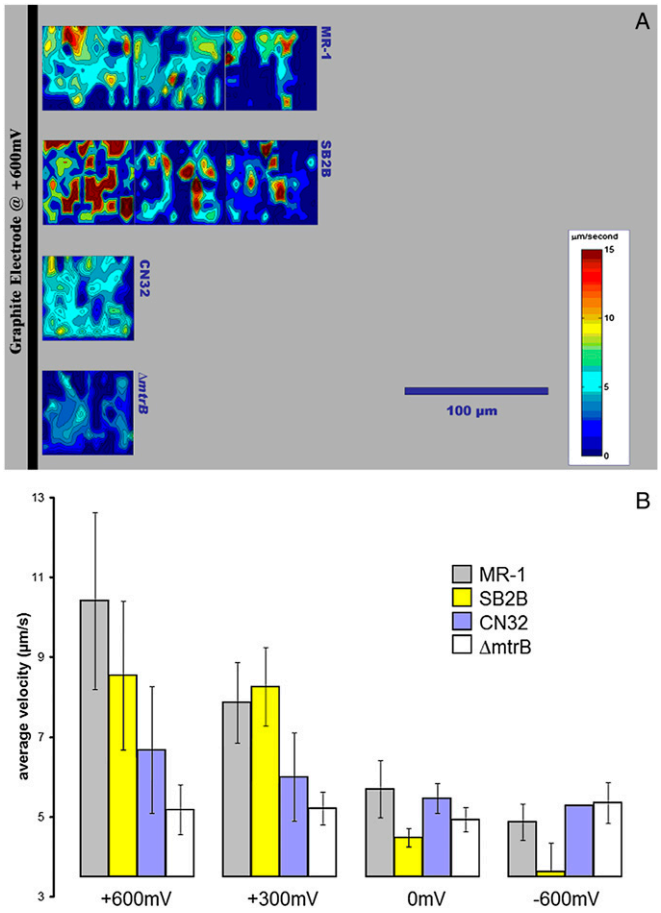

Fig. 3. Contour plots showing motility response of MR-1, SB2B, and CN32 strains, and the MR-1 Δ*mtrB* mutant to potentials applied to the working electrode in a microelectrochemical cell. (*A*) The digital contour plots show the average velocity near an electrode with applied potential (+600 mV) that mimics an electron-accepting surface like the anode of an MFC. The *x* and *y* axes correspond to horizontal and vertical screen positions from a number of 30-sec video clips, which are assembled in panoramic strips. The black bar on the left represents the location of the graphite electrode filament relative to each frame. These plots show results from four experiments with strains MR-1, SB2B, CN32, and Δ*mtrB,* which are displayed respectively from top to bottom in panoramic strips. The contour map shows regions of high bacterial velocity (red) and low velocity (blue). During the application of three positive potentials (+600, +300, and +150 mV) the wild-type bacteria responded with excited swimming near the electrode surface. (*B*) Average velocity values for the bacterial strains responding with 10 min of exposure to four different voltages (potentials) applied to the working electrode (+600 mV, +300 mV, 0 mV, and −600 mV). The graph compares wild types (MR-1, SB2B, and CN32) with the cytochrome deletion mutant, Δ*mtrB,* at each applied potential. The Δ*mtrB* mutant showed no swimming response throughout the range of positive and negative voltages. The swimming response of CN32 to small positive electric fields was relatively less than the responses of SB2B and MR-1. MR-1 and SB2B are considered to be good current-producing bacteria for an analogous MFC system. Error bars represent 2× standard deviation.

phenotype of the mutant. However, the results of the electrode experiments indicate that the CheA-3 chemotactic signal transduction pathway is not required for electrokinesis.

Previous studies have demonstrated that cells respond to strong electric fields according to their surface charge, in a response termed *galvanotaxis* (18–20), with cells showing defined trajectories and uniform movement toward an applied potential gradient, generated with a power supply, of 4 V/cm (18). Furthermore, application of electromagnetically induced electric fields was shown to promote motility while disrupting chemotaxis in *Escherichia coli* strains (21). In contrast, our study was designed to mimic the conditions that cells may encounter when using insoluble compounds for anaerobic respiration. In our study, with an applied potential of +600 mV the swimming velocity of MR-1 was enhanced in all directions of motion, rather than just in a single direction (Fig. 2*D*). Additionally, the motility response of MR-1 was dependent on the applied potential of the electrochemical cell. An applied potential of 0 mV (vs. graphite reference electrode) induced little cell response and short paths of motion (Fig. 2*C*), whereas an applied potential of +600 mV equivalent to 0.09 V/cm (vs. graphite reference electrode) induced high-velocity swimming and extended paths of motion (Fig. 2*D*, Fig. 3, and Movie S6). Higher applied potentials, of +1.2 V or more, interrupted all swimming: the cells followed a slow uniform migration more similar to the "defined trajectories" described by galvanotaxis. These results indicate that electrokinesis and galvanotaxis are different responses because the cell swimming patterns close to the electrode surfaces were distinct.

Electrokinesis in Other *Shewanella* Species. Electrokinetic responses were studied for two other *Shewanella* strains using both the MnO_2 particle and electrochemical cell electrode assays. *S. amazonensis* SB2B, which can generate comparable current to MR-1 in an MFC (Table 1), was found to exhibit strong electrokinesis around the MnO_2 particles, with a wider activity radius than MR-1 (Fig. 1*B* and Table 1). Around the electrode, the activity radius of SB2B was similar to that of MR-1 (Fig. 3*A* and Table 1), as was the average swimming velocity (Fig. 3*B*). Conversely, *S. putrefaciens* CN32, which generates less current than MR-1 in a MFC (Table 1), exhibited a spatially more confined motility response than MR-1 around both the MnO_2 particle (Fig. 1*B* and Table 1) and the electrode (Fig. 3*A* and Table 1). The average swimming speed of CN32 cells in response to +600 and +300 mV applied potentials was also lower than that of MR-1 and SB2B cells (Fig. 3*B*).

Kinetic Relaxation Time. With the electrode it was possible to perform experiments that could not be done with metal oxides, namely to vary the surface potential in an unobtrusive way and watch the response of the cells. Each evaluated wild-type strain showed a decrease in swimming speed when the applied potential was varied from +600 to −600 mV, although CN32 swimming speeds varied less than those of MR-1 and SB2B cells (Fig. 3*B*). In all cases the reduced speed was observed to occur within minutes after the potential was lowered. We refer to the period that cells continued to swim after the potential was decreased as the *relaxation time*. Strains SB2B and MR-1 were the most persistent swimmers after potentials were dropped (Fig. S2) (i.e., they had the longest relaxation times). When the potentials were varied in the positive direction, up to +600 mV, swimming speeds increased to previously observed levels.

Discussion

Electrokinesis: A Unique Behavioral Response? The behavioral response that we have termed electrokinesis was first observed as an excited motility response around MnO_2 particles (which have a positive redox potential in the range of +200–400 mV) under conditions in which the mineral was the only available electron acceptor. The response was also coincident with reduction of the electron acceptor. The more limited response to $Fe(OH)_3$ particles (which have a lower redox potential in the range of +100–300 mV) suggested that the bacteria respond to the presence of different solid phase electron acceptors, and that the redox potential of the electron acceptor may be an important component of this behavioral response. However, whereas the MnO_2 particles are likely to have a more positive redox potential than the $Fe(OH)_3$ particles, neither mineral used in our studies was extensively characterized. Thus, although electrokinesis may have a thermodynamic basis,

our experiments have not ruled out the possibility that the response could be based on the rate of flow of electrons to the minerals (because of their different surface characteristics and crystalline or amorphous structures) and thus have a kinetic basis.

Our experiments do show that electrokinesis is closely connected to the flow of electrons via EET because neither the Δ*cymA*, Δ*mtrA*, nor the Δ*mtrB* mutants showed electrokinesis in response to either MnO_2 particles or positive applied potentials in our electrochemical cell. Even more interesting was the observation that the motility response observed for the different *Shewanella* strains correlated not only with the redox potential of the electron acceptors used in the different experiments, but also with the current-generating ability of the strains, again suggesting that this unique response could have a kinetic basis. We do note that the electrokinetic response is similar to the chemokinetic response observed by Zhulin et al. (22), during studies on behavioral responses to oxygen in *Rhizobium meliloti*. These authors showed that *R. meliloti* responds to oxygen by increasing the swimming speed of cells and correlated this response with changes in proton motive force. Our preliminary studies with *S. oneidensis* MR-1 do not indicate a simple relationship between cell swimming speed and the redox potential of an electron acceptor. Swimming speeds of cells under anoxic conditions in the presence of nitrate [during NO^{3-} reduction to NO^{2-} (E_0' +430 mV)] and thiosulfate [during thiosulfate disproportionation (E_0' −400 mV)] were very similar (29.2 ± 11.2 μm/sec and 27.6 ± 18.4 μm/sec, respectively), whereas the swimming speed of cells in the presence of fumarate [during fumarate reduction to succinate (E_0' +30 mV)] was higher (38.4 ± 6.7 μm/sec). In future studies we will compare the reduction potential of different electron acceptors, the rates of electron acceptor reduction, and swimming speeds. These data will allow us to more clearly demonstrate whether *S. oneidensis* MR-1 shows chemokinetic responses to anaerobic electron acceptors and thus whether electrokinesis is a form of chemokinesis.

An important distinction between the behavioral responses to the soluble and insoluble electron acceptors used in this study is that whereas the soluble electron acceptors elicit a general response, the insoluble electron acceptors elicit only a localized response. These differences suggest that sensing, per se, is probably not involved in electrokinesis. In addition, the Δ*cheA-3* mutant, which is unable to sense soluble anaerobic electron acceptors, showed clear electrokinesis to positive applied potentials. However, our studies using the Δ*cheA-3* mutant did generate some contradictory data because the mutant cells did not localize around the MnO_2 particles. However, this lack of localization could have been due to the smooth-swimming phenotype of the mutant (i.e., a Δ*cheA-3* mutant cell would continually swim away from any touched particle). Galvanotaxis is a previously reported phenomenon (18–20) in which cells move toward strong electric fields (4 V/cm) with defined trajectories. The response is based on the surface charge of the cells. In contrast, our study used applied potentials to mimic the electron accepting conditions that cells may encounter in the environment. Under these conditions, the swimming velocity of MR-1 was enhanced *in all directions of motion*. Additionally, the motility response of MR-1 was dependent on the applied potential of the electrochemical cell. An applied potential of 0 mV (vs. graphite reference electrode) induced little cell response and short paths of motion, whereas an applied potential of +600 mV, equivalent to 0.09 V/cm (vs. graphite reference electrode), induced high-velocity swimming and extended paths of motion (Fig. 2 *C* and *D*, Fig. 3*B*, and Movie S6). Higher applied potentials of + 1.2 V (or more) interrupted all swimming: the cells followed a slow uniform migration more similar to the "defined trajectories" described by galvanotaxis. These results indicate that electrokinesis is distinct from galvanotaxis because the electric fields produced in our electrochemical system are very low, and there was no observed bacterial "front" that was attracted to the electrode surface.

The possibility that an extracellular electron shuttle plays a role in electrokinesis has not been ruled out. However, the effects of 1 mM AQDS (E_0' = −184 mV) on MR-1 (in increasing the number of cells swimming and in lengthening the relaxation time) suggest that, if the cells in our experiments were producing a shuttle, the concentration of this shuttle would be low. Many of the motile cells in both the MnO_2 and electrode experiments were, however, observed to transiently touch the surface of the electron acceptor but not to attach to the mineral or graphite surfaces (Movie S1 and Movie S6). Cells displaying this behavior could hypothetically be storing electrons on some biologic "capacitor," as suggested by Esteve-Núñez et al. (23), then rapidly discharging these electrons to the electron acceptor during these brief interaction events, and thus energizing the cell. If there is a kind of biologic capacitor, this might account for the different relaxation times observed for the different *Shewanella* strains. To this end, electrokinesis may require a combination of specialized electron storage/donating mechanisms by cells and efficient electron acceptor capacity by minerals. Our future research will explore whether electrokinesis has a thermodynamic or kinetic basis and will perform additional studies to determine whether the cells are indeed acting as biologic "capacitors."

Materials and Methods

Cultivation and Strains. *S. oneidensis* MR-1, *S. amazonensis* SB2B, *S. putrefaciens* CN32, and several mutants, originating from *S. oneidensis* MR-1, were tested in this study. Construction of the Δ*mtrB* (SO_1776) mutant was described previously (24, 14). The mutant is defective in metal oxide [Fe(III) oxide and MnO_2] reduction (12, 25) and current production in an MFC (13). To study the effects of interrupting electron flow from the cytoplasm to several terminal electron acceptors during anaerobic respiration, a *cymA* mutant (ORF SO_4591) that lacks a cytoplasmic membrane-bound, tetraheme *c*-type cytochrome, was tested (26–28). Additional screening of an *mtrA* (ORF SO_1777) mutant, deficient in periplasmic decaheme *c*-type cytochromes involved in Mn(IV) and Fe(III) reduction, allowed insight into the effects of cells deficient in terminal reductases (29–31). A mutant with a deletion in the central chemotaxis signal translocation pathway gene *cheA-3* (ORF SO_3207) was selected for its defective chemotaxis response (14).

All strains and mutants were grown aerobically on *Shewanella* Federation minimal medium with lactate (20 mM) for 48 h at 30°C (13). Five-milliliter aliquots of cells were harvested at optical density of 0.2–0.3 at 600 nm, then added to a buffered (50 mM Pipes) mixture of electron donor and acceptor. For any given chemical experiment the electron acceptor was either 10 mM fumarate, 10 mM thiosulfate, 5 mM nitrate, 1 mM AQDS, or 0.3 mM MnO_2. Subsamples containing cells and a mix of electron donor/acceptors were taken for the experiments and inoculated into anaerobic capillary tubes for in situ reduction experiments.

In Situ Metal Oxide Particle Reduction Experiments. Experiments with metal oxide reduction and other chemical electron acceptors were conducted in sealed, anaerobic, transparent capillary tubes (0.02 mm × 0.5 mm × 50 mm). The reduction process was observed under phase contrast (100×) using a Carl Zeiss Optical Microscope equipped with a Nikon digital camera, which captures video for desired intervals (usually 1–60 min).

In Situ Electrochemical Cell Experiments. Electrochemical experiments were conducted using a microelectrochemical device constructed from graphite fibers, transparent capillary tubes, and Nafion ion-exchange membranes (Fig. S1). Based on an MFC model (32), this system incorporates a graphite electrode into a thin glass, anaerobic capillary, which allows 100× light microscopy observation of cells during various applied potentials. The electrochemical cell was sterilized with 70% ethanol before the inoculation of bacterial cultures and then sealed with silicon vacuum grease during the experiments. The microbial suspension (without electron acceptor) was added directly to the apparatus within 1 h 15 min of being harvested from the aerobic culture to achieve equivalent dissolved oxygen content in solution. After device inoculation the system was allowed to settle for 25–30 min, and video data were then recorded. A potentiostat (Gamry Reference 600) was used to apply potentials to the graphite fiber working electrode internal to the electrochemical cell. Potentials were applied relative to a graphite electrode acting as a reference electrode in the cathode compartment. The cathode electrode was the counter electrode. Potentials were applied sequentially (vs. a graphite reference electrode) for the following time intervals after bacteria were

sealed into the system and allowed to establish equilibrium: (*i*) +600 mV applied for 30 min; (*ii*) +300 mV applied for 10 min; (*iii*) +150 mV applied for 10 min; (*iv*) 0 mV applied for 10 min; (*v*) −10 mV applied for 1 min; (*vi*) −30 mV applied for 1 min; (*vii*) −60 mV applied for 1 min; (*viii*) −150 mV applied for 10 min; (*ix*) −300 mV applied for 10 min; (*x*) −600 mV applied for 10 min; (*xi*) +600 mV applied for 30 min; (*xii*) 0 mV applied for 10 min; (*xiii*) −150 mV applied for 10 min; and (*xiv*) −300 mV applied for 10 min.

Video data were collected during all cycles, with the field of view focused on the edge of the working electrode. Video data were captured during several key phases with each of the applied potentials shown above. The first video recording captured the open circuit phase, which occurred before the initial application of any potential. Then after applied potential, video was continuously recorded for the next 1 min (for all applied potentials *i*–*xiii*), then recorded at 5 min, 10 min (for all potential intervals excluding *v*–*vii*), and 30 min (for potential intervals *i* and *xi*). Only the results from the video data collected during the potential intervals *i*, *ii*, *iv*, *x*, and *xi* (from list) have been included in this study.

Tracking Cell Movements. Cells were monitored near metal oxides and working electrodes in electrochemical cells, using 100× light microscopy (33). The locations of individual cells and the subsequent linking of these locations to form trajectories are based on the particle tracking algorithms of Crocker et al. (34). Briefly, individual frames were captured digitally at ≈29 frames per second and processed with a spatial band pass filter to generate high-contrast images of bacteria. Each image was reduced to a matrix of numeric pixel values. A peak finding algorithm located all of the intensity peaks (bacteria) that were above a given set threshold. The peak locations were linked to form trajectories by seeking the most probable set of interframe associations. Motility indicators, such as the average cellular velocity, were subsequently computed from the complete trajectories. We used a MATLAB (The Mathworks) implementation of the tracking algorithms (http://physics.georgetown.edu/matlab/). The computed trajectories were then checked manually by visual inspection and compared with video tracked by hand, frame by frame. The algorithm parameters (expected cell size, minimum spot intensity, and maximum distance traveled between frames) were adjusted to obtain tracking with an acceptable level of accuracy. For this study, the acceptable level was achieved by the program only if it could successfully detect and assign trajectories to all well-photographed bacteria, which are in focus and have sharp contrast with background, as well as most out-of-focus bacteria (>75%) in all collected video samples.

From our analysis of *Shewanella* motility, it is worth noting that individual cells are capable of swimming significantly faster than the average velocity, because the average velocity takes into account all bacteria in each frame, including many slow-moving or near-stationary cells. For example, Fig. S3*A* and *B* feature velocity vs. time traces for all of the cells tracked during a 10-sec interval, at 0 mV and +600 mV working electrode bias, respectively. Although an increase in high-velocity events at +600 mV is clearly evident, there are many slow-moving ones (below 10 μm/s) under both bias conditions.

The term *activity radius* was evoked to quantify the extent of the bacterial "swarm" surrounding an electron acceptor during the initial 0.5–1.5 h after exposure, which was estimated using the following procedure. First the panorama composites of motility, shown in Fig. 1*B* and Fig 3*A*, were assembled from the output of multiple consecutive video data samples. From each experiment, the overall swimming activity within the video frame, equivalent to 48 μm × 64 μm field of view, was most accurately characterized by the sum of all velocity magnitudes through 10 sec of video data. The first video in the series captured the bacterial swimming in the field of view immediately adjacent to the solid acceptor, then by adjusting the microscope stage in the positive *x* direction by +64 μm, the next field of view just to the right of the previous video frame was captured and analyzed. This step was repeated until all possible elevated activity was evaluated. From analyses of these panorama video and data outputs the activity radius was said to be the distance (in micrometers) from the solid acceptor to the right edge of the frame where the swimming activity fell below ≈25% of the overall swimming activity level detected in the first video data in the series. Alternatively, the activity radius was defined as the distance from the solid acceptor to the right edge of the video frame where the motility level decreased below the level detected in a nonstimulated, nonswimming sample captured within the same experiment and time constraints.

ACKNOWLEDGMENTS. We thank Norman Harris for consultation and collaboration on material science matters; Lewis Hsu and Gijs Kuenen for advice on experimental design and methods; Frank Corsetti and Mike Waters for assistance with microscopy techniques and setups; John Petruska and Arieh Warshel for advice about theoretical modeling and field strength estimations; Jun Li for supplying the Δ*cheA*-3 mutant; and Samantha Reed and David Culley for supplying the Δ*mtrB*, Δ*mtrA*, and Δ*cymA* mutants. Supported by the Department of Energy, and Department of Defense Multidisciplinary University Research Initiative Award FA9550-06-1-0292. M.J.W. is funded by the National Science Foundation.

1. Fredrickson JK, et al. (2008) Towards environmental systems biology of *Shewanella*. *Nat Rev Microbiol* 6:592–603.
2. Lovley DR, Coates JD, Blunt-Harris EL, Phillips EJP, Woodward JC (1996) Humic substances as electron acceptors for microbial respiration. *Nature* 382:445–448.
3. Schröder U (2007) Anodic electron transfer mechanisms in microbial fuel cells and their energy efficiency. *Phys Chem Chem Phys* 9:2619–2629.
4. Kim BH, Kim HJ, Hyun MS, Park DH (1999) Direct electrode reaction of Fe (III)-reducing bacterium, *Shewanella putrefaciens*. *J Microbiol Biotechnol* 9:127–131.
5. Newman DK, Kolter R (2000) A role for excreted quinones in extracellular electron transfer. *Nature* 405:94–97.
6. Marsili E, et al. (2008) *Shewanella* secretes flavins that mediate extracellular electron transfer. *Proc Natl Acad Sci USA* 105:3968–3973.
7. von Canstein H, Ogawa J, Shimizu S, Lloyd JR (2008) Secretion of flavins by *Shewanella* species and their role in extracellular electron transfer. *Appl Environ Microbiol* 74:615–623.
8. Myers CR, Myers JM (1992) Localization of cytochromes to the outer membrane of anaerobically grown *Shewanella putrefaciens* MR-1. *J Bacteriol* 174:3429–3438.
9. Reguera G, et al. (2005) Extracellular electron transfer via microbial nanowires. *Nature* 435:1098–1101.
10. Gorby YA, et al. (2006) Electrically conductive bacterial nanowires produced by *Shewanella oneidensis* strain MR-1 and other microorganisms. *Proc Natl Acad Sci USA* 103:11358–11363.
11. El-Naggar MY, Gorby YA, Xia W, Nealson KH (2008) The molecular density of states in bacterial nanowires. *Biophys J* 95:L10–L12.
12. Beliaev AS, Saffarini DA (1998) *Shewanella putrefaciens mtrB* encodes an outer membrane protein required for Fe(III) and Mn(IV) reduction. *J Bacteriol* 180:6292–6297.
13. Bretschger O, et al. (2007) Current production and metal oxide reduction by *Shewanella oneidensis* MR-1 wild type and mutants. *Appl Environ Microbiol* 73:7003–7012.
14. Li J, Romine MF, Ward MJ (2007) Identification and analysis of a highly conserved chemotaxis gene cluster in *Shewanella* species. *FEMS Microbiol Lett* 273:180–186.
15. Nealson KH, Moser DP, Saffarini DA (1995) Anaerobic electron acceptor chemotaxis in *Shewanella putrefaciens*. *Appl Environ Microbiol* 61:1551–1554.
16. Bencharit S, Ward MJ (2005) Chemotactic responses to metals and anaerobic electron acceptors in *Shewanella oneidensis* MR-1. *J Bacteriol* 187:5049–5053.
17. Lies DP, et al. (2005) *Shewanella oneidensis* MR-1 uses overlapping pathways for iron reduction at a distance and by direct contact under conditions relevant for Biofilms. *Appl Environ Microbiol* 71:4414–4426.
18. Shi W, Stocker BA, Adler J (1996) Effect of the surface composition of motile *Escherichia coli* and motile *Salmonella* species on the direction of galvanotaxis. *J Bacteriol* 178:1113–1119.
19. Murray JLS, Jumars PA (2002) Clonal fitness of attached bacteria predicted by analog modeling. *Bioscience* 52:343–355.
20. Ogawa N, Oku H, Hashimoto K, Ishikawa M (2005) Microrobotic visual control of motile cells using high-speed tracking system. *IEEE Trans Robot* 21:704–712.
21. Eisenbach M, Zimmerman JE, Ciobotariu A, Fischler H, Korenstein R (1983) Electric field effects on bacterial motility and chemotaxis. *Bioelectrochem Bioenerg* 10:499–510.
22. Zhulin IB, Lois AF, Taylor BL (1995) Behavior of *Rhizobium meliloti* in oxygen gradients. *FEBS Lett* 367:180–182.
23. Esteve-Núñez A, Sosnik J, Visconti P, Lovley DR (2008) Fluorescent properties of *c*-type cytochromes reveal their potential role as an extracytoplasmic electron sink in *Geobacter sulfurreducens*. *Environ Microbiol* 10:497–505.
24. Marshall MJ, et al. (2006) *c*-type cytochrome-dependent formation of U(IV) nanoparticles by *Shewanella oneidensis*. *PLoS Biol* 4:e268.
25. Myers CR, Myers JM (2002) MtrB is required for proper incorporation of the cytochromes OmcA and OmcB into the outer membrane of *Shewanella putrefaciens* MR-1. *Appl Environ Microbiol* 68:5585–5594.
26. Myers CR, Myers JM (1997) Cloning and sequence of *cymA*, a gene encoding a tetraheme cytochrome *c* required for reduction of iron(III), fumarate, and nitrate by *Shewanella putrefaciens* MR-1. *J Bacteriol* 179:1143–1152.
27. Myers JM, Myers CR (2000) Role of the tetraheme cytochrome CymA in anaerobic electron transport in cells of *Shewanella putrefaciens* MR-1 with normal levels of menaquinone. *J Bacteriol* 182:67–75.
28. Schwalb C, Chapman SK, Reid GA (2002) The membrane-bound tetrahaem *c*-type cytochrome CymA interacts directly with the soluble fumarate reductase in *Shewanella*. *Biochem Soc Trans* 30:658–662.
29. Pitts KE, et al. (2003) Characterization of the *Shewanella oneidensis* MR-1 decaheme cytochrome MtrA: Expression in *Escherichia coli* confers the ability to reduce soluble Fe(III) chelates. *J Biol Chem* 278:27758–27765.
30. Beliaev AS, et al. (2005) Global transcriptome analysis of *Shewanella oneidensis* MR-1 exposed to different terminal electron acceptors. *J Bacteriol* 187:7138–7145.
31. Bencheikh-Latmani R, et al. (2005) Global transcriptional profiling of *Shewanella oneidensis* MR-1 during Cr(VI) and U(VI) reduction. *Appl Environ Microbiol* 71:7453–7460.
32. Manohar AK, Bretschger O, Nealson KH, Mansfeld F (2008) The polarization behavior of the anode in a microbial fuel cell. *Electrochim Acta* 53:3508–3513.
33. Vaituzis Z, Doetsch RN (1969) Motility tracks: Technique for quantitative study of bacterial movement. *Appl Environ Microbiol* 17:584–588.
34. Crocker JC, Grier DG (1996) Methods of digital video microscopy for colloidal studies. *J Colloid Interface Sci* 179:298–310.